Journal of Molecular Structure 1139 (2017) 209–221

Contents lists available at ScienceDirect

Journal of Molecular Structure

journal homepage: http://www.elsevier.com/locate/molstruc

Synthesis and supramolecular self-assembly of thioxothiazolidinone derivatives driven by H-bonding and diverse π–hole interactions: A combined experimental and theoretical analysis

Hina Andleeb [a], Imtiaz Khan [a], Antonio Bauzá [b], Muhammad Nawaz Tahir [c], Jim Simpson [d], Shahid Hameed [a, **], Antonio Frontera [b, *]

[a] Department of Chemistry, Quaid-i-Azam University, Islamabad, 45320, Pakistan
[b] Departament de Química, Universitat de les Illes Balears, Crta. de Valldemossa km 7.5, 07122, Palma de Mallorca, Baleares, Spain
[c] Department of Physics, University of Sargodha, Sargodha, 40100, Pakistan
[d] Department of Chemistry, University of Otago, P.O. Box 56, Dunedin, 9054, New Zealand

ARTICLE INFO

Article history:
Received 8 November 2016
Received in revised form
6 March 2017
Accepted 11 March 2017
Available online 13 March 2017

Keywords:
Thioxothiazolidinone
Noncovalent interactions
π–hole interactions
Theoretical analysis

ABSTRACT

Two new 3-aryl-5-(4-nitrobenzylidene)-2-thioxothiazolidin-4-one derivatives (**1** & **2**) were synthesized by the Knoevenagel condensation reaction of 3-(4-aryl)-2-thioxo-1,3-thiazolidin-4-ones with 4-nitrobenzaldehyde. Both products were isolated as orange crystalline solids in good yields and were fully characterized by analytical, spectroscopic and structural methods. The interesting supramolecular assemblies of the title compounds observed in the solid state were analyzed by Density Functional Theory (DFT) calculations (M06-2X/def2-TZVP), Molecular Electrostatic Potential (MEP) surfaces and characterized by means of the Bader's theory of "atoms-in-molecules" (AIM) and NCIplot. The computation of the energy features of the diverse noncovalent interactions including C–H···π, π···π and lp···π-hole interactions revealed their conspicuous role in the stabilization of the three-dimensional supramolecular frameworks for both compounds in addition to the C–H···O/S H-bonding interactions.

1. Introduction

Rhodanine, a five-membered heterocyclic skeleton, represents a very important scaffold in the drug discovery arena with widespread applications [1,2]. This pharmacophore (2-thioxo-1,3-thiazolidin-4-one) has demonstrated multiple biological inhibitory activities [3] including aldose reductase [4], HCV NS3 protease [5], β-lactamase [6], *N*-acetyltransferase [7], histone acetyltransferase [8], and histidine decarboxylase [9]. The 1,3-thiazolidin-4-one core is also an essential pharmacophore for the treatment of type 2 diabetes and is found in several drugs such as Epalrestat, Rosiglitazone, Pioglitazone, and Ciglitazone [10]. Rhodanine derivatives, modified at the methylene group (ylidenerhodanines), exhibit antibacterial [11], antifungal [12–14], and anticancer activities [15]. These versatile building blocks also find potential applications in the synthesis of compounds with antitumor [16–18], and anti-HIV properties [19,20]. In addition, rhodanine derivatives have diverse applications in industry and coordination chemistry [21]. Moreover, the use of rhodanine compounds as a dye sensitizer [22], and in the synthesis of non-linear optical (NLO) materials [23,24] attests to the broad utility of this framework.

The foundation of molecular recognition processes and crystal growth is a concert of intermolecular interactions. Consequently a proper understanding of these noncovalent interactions is crucial to many fields related to supramolecular chemistry and self-assembly processes. The shared physical basis of well-known forces such as hydrogen and halogen bonding interactions [25–28] is that electron rich entities interact with a so-called "σ-hole", which is defined as a positive electrostatic potential along the vector of a covalent bond (X–H or X–I) [29–31]. In addition, positive electrostatic potentials can also be found in electron-deficient π-systems and these so-called "π-holes" [32–35] can also interact with electron-rich species in a directional fashion in the solid state [32,36,37]. In fact some of us have recently shown that this reasoning applies to π-holes in common nitro-compounds such as

* Corresponding author.
** Corresponding author.
E-mail addresses: shameed@qau.edu.pk (S. Hameed), toni.frontera@uib.es (A. Frontera).

http://dx.doi.org/10.1016/j.molstruc.2017.03.046
0022-2860/

nitromethane and nitroaromatics [32], and also other less common nitro-bearing molecules such as nitrate esters [38].

In this manuscript, we report the convenient synthesis (four steps) and X-ray characterization of two thioxothiazolidinone derivatives (Scheme 1) that exhibit interesting solid state architectures. Apart from the conventional C–H···O/S H-bonding interactions (σ-hole interactions), π-hole interactions involving the π-acidic five-membered ring and the nitro groups are also relevant to rationalize the overall crystal packing of compounds **1** and **2**. These interactions have been studied using high level DFT calculations (M06-2X/def2-TZVP) and the Bader's theory of atoms in molecules. The computations and crystal structures reported in this work support the concept that π-hole interactions with nitrocompounds are directional and relevant in crystal engineering.

2. Experimental and theoretical methods

2.1. Substrates and reagents

p-Anisidine, *p*-toluidine and ethylenediamine were from Merck. 4-Nitrobenzaldehyde was purchased from Sigma Aldrich. The reagents used were of analytical grade. Ethanol, chloroform and methanol were supplied by Lab scan (Patuman, Bankok). Dichloromethane and diethyl ether were products from Riedel de Haen (Seezle) while ethyl acetate and acetone were obtained from local commercial sources. All solvents used were either anhydrous or dried and purified by passage through activated alumina columns under nitrogen pressure.

2.2. Instrumentation

Unless specified otherwise, all reactions were carried out using oven-dried glassware. The reaction progress was monitored by thin layer chromatography (TLC) using Merck DF-Alufoilien $60F_{254}$ 0.2 mm precoated plates. Compounds were visualized by exposure to UV light at 254 nm. Melting points were recorded in open capillaries using a Gallenkamp melting point apparatus (MP-D) and are uncorrected. FTIR spectra were recorded on a Thermoscientific Fourier Transform Infra-Red Spectrophotometer USA model Nicolet 6700 using the attenuated total refraction (ATR) technique. NMR spectra were acquired on Bruker AV300 spectrometer at room temperature. ^{1}H and ^{13}C NMR spectra were referenced to external tetramethylsilane *via* the residual protonated solvent (^{1}H) or the solvent itself (^{13}C). All chemical shifts are reported in parts per million (ppm). For $CDCl_3$, shifts are referenced to 7.27 ppm for ^{1}H NMR spectroscopy and 77.0 ppm for ^{13}C NMR spectroscopy. For DMSO-d_6, shifts are referenced to 2.50 ppm for ^{1}H NMR spectroscopy and 39.97 ppm for ^{13}C NMR spectroscopy. Coupling constant (*J*) values are reported to the nearest 0.5 Hz. Elemental analyses were performed on a Leco CHNS-932 Elemental Analyzer, Leco Corporation (USA).

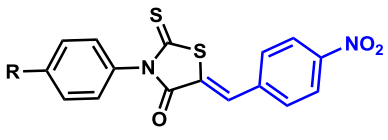

1: R = OMe
2: R = Me

Scheme 1. Compounds 1–2.

2.3. Synthesis

2.3.1. Preparation of 3-(4-substituted phenyl)-2-thioxothiazolidin-4-one (9 & 10)

Carbon disulfide (0.2 mol) in diethyl ether (50 mL) was added dropwise to a suspension of the corresponding aniline (**3** & **4**) (0.1 mol) and triethylamine (0.2 mol) in a 250 mL round bottom flask at 0 °C. The reaction mixture was stirred at the same temperature for 5–6 h. After complete precipitation, the corresponding triethylammonium dithiocarbamate (**5** & **6**) was filtered *in vacuo* and washed with diethyl ether. The solid product was used in the next step without further purification.

A solution of the corresponding triethylammonium dithiocarbamate (**5** & **6**) (0.1 mol) in water/ethanol (1:1) was added slowly to a stirred solution of sodium chloroacetate (0.1 mol) in H_2O (35 mL) and the resulting mixture was stirred at 70 °C. After completion of the reaction (monitored by TLC), the mixture was cooled to room temperature and slowly poured into boiling hydrochloric acid (12 M, 40 mL). After 5 min, the solution was allowed to cool slowly to room temperature to precipitate the desired 3-(4-substituted phenyl)-2-thioxothiazolidin-4-one derivatives (**9** & **10**). The precipitated solid was filtered and washed with water followed by cold ethanol, dried and recrystallized from ethanol [39]. The spectroscopic data were consistent with those reported in literature [40].

2.3.2. Preparation of 3-aryl-5-(4-nitrobenzylidene)-2-thioxothiazolidin-4-one (1 & 2)

To a stirred solution of an appropriate 3-(4-substituted phenyl)-2-thioxothiazolidin-4-one (**9** & **10**) (1.0 mmol) in chloroform/methanol (8:1; 18 mL), glacial acetic acid (40 mmol, 2.28 mL) was added followed by ethylenediamine (0.2 mmol, 11 μL). The resulting mixture was stirred for 15 min followed by the addition of 4-nitrobenzaldehyde (1.2 mmol) at ambient temperature. After completion of the reaction (TLC; 40% acetone/petroleum ether), the excess solvent was removed to afford a bright yellow solid. The crude solid was washed with methanol/water (10:1), filtered, dried and recrystallized (chloroform/methanol; 1:6) to yield the title compounds (**1** & **2**) [39].

2.3.2.1. (Z)-3-(4-methoxyphenyl)-5-(4-nitrobenzylidene)-2-thioxothiazolidin-4-one (1). Orange crystals (79%): m.p 268–269 °C; R_f: 0.31 (40% acetone/*n*-hexane); IR (ATR, cm^{-1}): 3085 (Ar–H), 2994, 2853 (CH_3), 1598 (C=O), 1565, 1521 (C=C), 1363 (C=S); ^{1}H NMR (300 MHz, DMSO-d_6): δ 8.38 (2H, d, *J* = 8.7 Hz, ArH), 7.96 (2H, d, *J* = 8.7 Hz, ArH), 7.95 (1H, s, =CH–ArNO_2), 7.36–7.32 (2H, m, ArH), 7.12–7.09 (2H, m, ArH), 3.83 (3H, s, OCH_3); ^{13}C NMR (75 MHz, DMSO-d_6): δ 194.29 (C=S), 167.30 (C=O), 160.28, 148.08, 139.72, 131.91, 130.32, 129.86, 128.21, 127.78, 124.94, 115.03, 55.91. Anal. Calcd. for $C_{17}H_{12}N_2O_4S_2$ (372.02): C, 54.83; H, 3.25; N, 7.52; S, 17.22%; found: C, 54.66; H, 3.04; N, 7.30; S, 17.05%.

2.3.2.2. (Z)-5-(4-nitrobenzylidene)-2-thioxo-3-(p-tolyl)thiazolidin-4-one (2). Orange crystals (83%): m.p 273–274 °C; R_f: 0.45 (40% acetone/*n*-hexane); IR (ATR, cm^{-1}): 3076 (Ar–H), 2989, 2832 (CH_3), 1597 (C=O), 1564, 1519 (C=C), 1365 (C=S); ^{1}H NMR (300 MHz, $CDCl_3$): δ 8.38 (2H, d, *J* = 8.7 Hz, ArH), 7.81 (1H, s, =CH–ArNO_2), 7.76 (2H, d, *J* = 8.7 Hz, ArH), 7.40 (2H, d, *J* = 8.1 Hz, ArH), 7.19 (2H, d, *J* = 8.1 Hz, ArH), 2.47 (3H, s, CH_3); ^{13}C NMR (75 MHz, DMSO-d_6): δ 192.29 (C=S), 172.30 (C=O), 167.28, 140.28, 139.30, 131.73, 130.98, 130.46, 129.55, 128.00, 127.90, 124.53, 21.44. Anal. Calcd. for $C_{17}H_{12}N_2O_3S_2$ (356.03): C, 57.29; H, 3.39; N, 7.86; S, 17.99%; found: C, 57.03; H, 3.20; N, 7.62; S, 17.71%.

2.4. Crystal growth development

Good quality single crystals of compounds **1** and **2** suitable for X-ray diffraction analysis were grown from 10% $CHCl_3$:EtOH solutions by slow evaporation at ambient temperature.

2.5. Single crystal data collection and structure solution

The X-ray measurements for compounds **1** and **2** (Table 1) were carried out on a Bruker APEXII Kappa CCD single crystal diffractometer equipped with a graphite monochromator. Mo-Kα radiation (λ = 0.71073 Å) was used for the collection, which was controlled by APEX2 [41] with data collected at 296(2)K. Data were corrected for Lorentz and polarization effects using SAINT [41] and multi-scan absorption corrections were applied using SADABS [41]. The structures were solved by direct methods using SHELXS-97 [42] and refined using full-matrix least-squares procedures with SHELXL-2014 [43]. All non-hydrogen atoms were refined anisotropically and all hydrogen atoms bound to carbon were placed in the calculated positions, and their thermal parameters were refined isotropically with Ueq = 1.2 or 1.5 Ueq(C). The molecular plots and packing diagrams were drawn using Mercury [44] and additional metrical data were calculated using PLATON [45]. Tabular material was prepared using WINGX [46].

2.6. Theoretical methods

Calculations of the noncovalent interactions were carried out using TURBOMOLE version 7.0 [47] using the M06-2X/def2-TZVP level of theory. To evaluate the interactions in the solid state, we have used the crystallographic coordinates. This procedure and level of theory have been successfully used to evaluate similar interactions [48]. We have also computed two assemblies using the MP2/def2-TZVP level of theory and the binding energies are comparable to those computed using the M06-2X functional, thus giving reliability to the level of theory used herein. The interaction energies were computed by calculating the difference between the energies of isolated monomers and their assembly. The interaction energies were corrected for the Basis Set Superposition Error (BSSE) using the counterpoise method [49]. The Bader's "Atoms in molecules" theory [50] has been used to study the interactions discussed herein by means of the AIMall calculation package [51]. For the calculation of the MEP (Molecular Electrostatic Potential) surfaces we have used the SPARTAN10 software [52]. The NCI plot is a visualization index based on the electron density and its derivatives, and enables identification and visualization of non-covalent interactions efficiently. The isosurfaces correspond to both favorable and unfavorable interactions, as differentiated by the sign of the second density Hessian eigenvalue and defined by the isosurface color. NCI analysis allows an assessment of host-guest complementarity and the extent to which weak interactions stabilize a complex. The information provided by NCI plots is essentially qualitative, i.e. which molecular regions interact. The color scheme is a red-yellow-green-blue scale with red for ρ^{+}_{cut} (repulsive) and blue for ρ^{-}_{cut} (attractive). Yellow and green surfaces correspond to weak repulsive and weak attractive interactions, respectively [53].

Table 1
Crystal data and structure refinement for (**1**) and (**2**).

Data	Compound 1	Compound 2
Empirical formula	$C_{17}H_{12}N_2O_4S_2$	$C_{17}H_{12}N_2O_3S_2$
Formula weight	372.41	356.41
Temperature	296(2) K	296(2) K
Wavelength	0.71073 Å	0.71073 Å
Crystal system	Triclinic	Triclinic
Space group	P -1	P -1
Unit cell dimensions	a = 4.2172(4) Å	a = 7.3942(8) Å
	b = 12.3528(11) Å	b = 8.0203(9) Å
	c = 16.6547(16) Å	c = 15.2417(18) Å
	α = 106.097(5)°	α = 78.332(4)°
	β = 94.489(5)°	β = 83.687(4)°
	γ = 95.340(5)°	γ = 66.940(4)°
Volume	825.05(14) $Å^3$	814.00(16) $Å^3$
Z	2	2
Density (calculated)	1.499 Mg/m^3	1.454 Mg/m^3
Absorption coefficient	0.348 mm^{-1}	0.345 mm^{-1}
F(000)	384	368
Crystal size	0.42 × 0.18 × 0.16 mm^3	0.40 × 0.32 × 0.16 mm^3
Theta range for data collection	1.728–27.475°	2.803–27.000°
Index ranges	−5 = h<=5,	−9 = h<=9,
	−15 = k<=14,	−10 = k<=10,
	−20 = l<=21	−19 = l<=19
Reflections collected	12988	12986
Independent reflections	3703 [R(int) = 0.0423]	3524 [R(int) = 0.0447]
Completeness to theta = 25.242°	99.8%	99.5%
Refinement method	Full-matrix least-squares on F^2	Full-matrix least-squares on F^2
Data/restraints/parameters	3703/0/227	3524/0/218
Goodness-of-fit on F^2	1.024	1.068
Final R indices [I > 2sigma(I)]	R^1 = 0.0475,	R^1 = 0.0675,
	wR^2 = 0.1057	wR^2 = 0.1848
R indices (all data)	R^1 = 0.0793,	R^1 = 0.0882,
	wR^2 = 0.1195	wR^2 = 0.2090
Largest diff. peak and hole	0.291 and −0.210 e.$Å^{-3}$	0.848 and −0.292 e.$Å^{-3}$
CCDC	1491798	1491799

3. Results and discussion

3.1. Synthesis and spectroscopic characterization

Synthesis of rhodanine compounds (**1** & **2**) was accomplished by the synthetic route illustrated in Scheme 2. Triethylammonium *N*-aryl dithiocarbamates (**5** & **6**) were prepared by reaction of the corresponding aniline (*p*-anisidine/*p*-toluidine) (**3** & **4**) (1.0 equiv) with carbon disulfide (2.0 equiv) in diethyl ether under basic conditions (triethylamine; 2.0 equiv) which subsequently afforded the sodium 2-(*N*-4-substituted phenylcarbamothioylthio)acetates (**7** & **8**) from a reaction with sodium chloroacetate in ethanol/water (1:1). The 3-aryl-2-thioxo-1,3-thiazolidin-4-ones (**9** & **10**) were synthesized by cyclization of **7** and **8** in boiling hydrochloric acid [39].

Knoevenagel condensation reactions of 3-(4-aryl)-2-thioxo-1,3-thiazolidin-4-ones (**9** & **10**) with 4-nitrobenzaldehyde gave 3-aryl-5-(4-nitrobenzylidene)-2-thioxothiazolidin-4-ones (**1** & **2**) in good yield [39].

The structures of the synthesized compounds (**1** & **2**) were characterized by the usual analytical techniques including FT-IR, ^{1}H and ^{13}C NMR spectroscopy. In the IR spectra, typical stretching vibrations for the C=O and C=S moieties were found around 1598–1597 and 1365–1363 cm^{-1}, respectively. Distinct C_{sp2}-H stretching vibrations were observed in the region 3085–3076 cm^{-1}.

In ^{1}H NMR spectra, the lone olefinic proton (=C–H) resonated as a singlet at 7.95–7.81 ppm confirming the *Z*-configuration for the exocyclic double bond as evident from literature [54–57]. In addition, M06-2X/def2-TZVP calculations confirm that the *Z* isomer is 5.7 kcal/mol more stable than the *E* one. The reason for this deshielding is attributed to the *cis* position of the carbonyl oxygen of the rhodanine ring to the =CH and hence the *Z* configuration. The *cis* positioning is due to the high degree of thermodynamic stability of these compounds because of the intramolecular hydrogen bond that can be formed between the hydrogen atom of =CH and the oxygen atom in rhodanine [52].

This distinctive feature was further confirmed by the single crystal X-ray diffraction analysis (*vide infra*). The structures (**1** & **2**) were further identified by ^{13}C NMR spectroscopy where diagnostic chemical shifts around 194–192 ppm were attributed to the presence of C=S groups in the rhodanine rings, whereas the C=O functional group resonance was found at 172–167 ppm. Finally, the purity of the synthesized compounds **1** and **2** was determined by elemental analysis.

3.2. Molecular structures of (Z)-3-(4-methoxyphenyl)-5-(4-nitrobenzylidene)-2-thioxothiazolidin-4-one (1) and (Z)-5-(4-nitrobenzylidene)-2-thioxo-3-(p-tolyl)thiazolidin-4-one (2)

The molecular structures of both compounds (Fig. 1) are sufficiently similar to be discussed together, with each molecule comprising a central 2-thioxo-1,3-thiazolidin-4-one ring system with phenyl substituents on the thiazolidine N3 atoms and 4-nitrobenzylidene substituents on C5. The molecules differ only in the nature of the substituents on the 4-positions of the two phenyl rings with a methoxy group in **1** and a methyl group for **2**. Selected bond distances and angles are shown in Table S1 (ESI). Both molecules adopt a *Z*-configuration about the C5=C6 double bond. In both molecules, the 4-nitrobenzylidene-2-thioxo-1,3-thiazolidin-4-one segments of the molecules are surprisingly planar, no doubt imposed in part by intramolecular C8–H8···S1 hydrogen bonds in both molecules, Tables 2 and 3. The root mean square deviations are 0.0678 Å for **1** and 0.0728 Å for **2** from the best fit planes through all 17 non-hydrogen atoms of these moieties. This planarity is underscored further by the fact that the 1,3-thiazolidine and its adjacent phenyl ring are inclined at angles of 6.21(13)° for **1** and 7.90(8)° for **2**. Additional evidence is provided by the corresponding inclinations of this phenyl ring and its nitro substituent, which are 4.1(4)° and 5.2(3)° respectively.

In contrast, the N bound phenyl ring subtends an angle of 60.13(6)° to the thiazolidine ring for **1** and is almost orthogonal to it in **2** with a dihedral angle 82.75(11)°. The methoxy substituent in **1** lies close to the plane of its benzene ring with an angle of 1.5(3)° between the benzene ring plane and the plane containing C16, O16 and C161.

Nine structures of molecules with a central 2-thioxo-1,3-

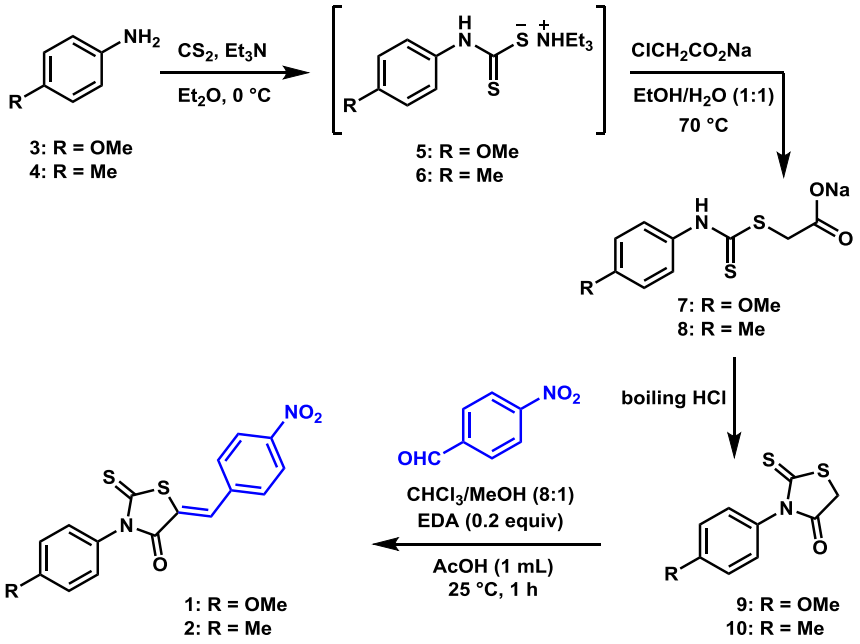

Scheme 2. Synthesis of 3-aryl-5-(4-nitrobenzylidene)-2-thioxothiazolidin-4-ones (1 & 2).

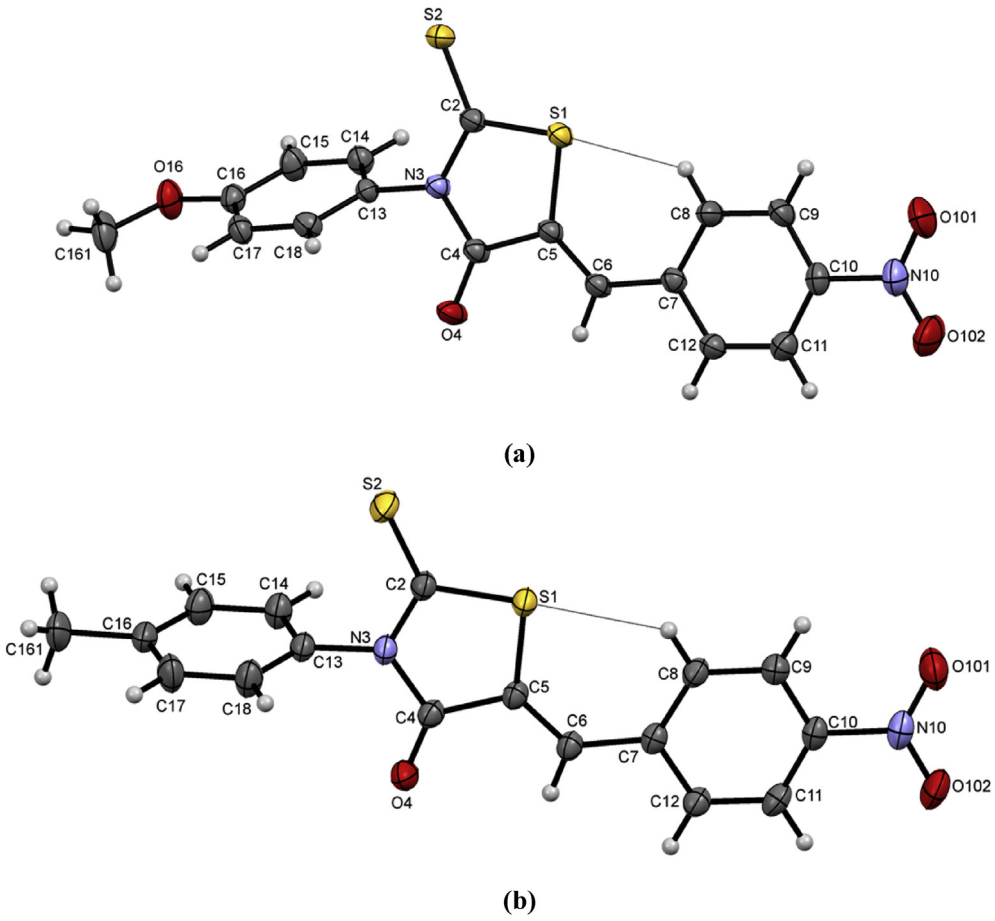

Fig. 1. The molecular structures of (**a**) compound **1** and (**b**) compound **2** with displacement ellipsoids drawn at the 50% probability level. Intramolecular hydrogen bonds are drawn as dotted lines.

Table 2
Hydrogen bonds for **1** [Å and °].

D–H … A	d(D–H)	d(H … A)	d(D … A)	<(DHA)
C(8)–H(8) … S(1)	0.93	2.51	3.223(3)	134
C(6)–H(6) … O(4)#1	0.93	2.47	3.354(3)	159.8
C(12)–H(12) … O(4)#1	0.93	2.56	3.416(3)	152.7
C(8)–H(8) … S(2)#2	0.93	2.92	3.580(3)	129.0
C(9)–H(9) … S(2)#2	0.93	2.99	3.608(3)	125.0
C(15)–H(15) … O(16)#3	0.93	2.49	3.417(3)	174.6
C(161)-H(16B) … O(101)#4	0.96	2.63	3.151(4)	114.7
C(18)–H(18) … O(4)#5	0.93	2.52	3.294(3)	140.4

Symmetry transformations used to generate equivalent atoms: #1 −x+1,−y,-z+1 #2 −x,−y+1,-z+1 #3 −x,−y,−z #4 x−2,y−1,z−1 #5 x−1,y,z.

Table 3
Hydrogen bonds for **2** [Å and °].

D–H … A	d(D–H)	d(H … A)	d(D … A)	<(DHA)
C(8)–H(8) … S(1)	0.93	2.54	3.250(3)	133
C(18)–H(18) … O(102)#2	0.93	2.53	3.432(4)	163.2
C(9)–H(9) … O(4)#3	0.93	2.52	3.293(4)	141.1
C(14)–H(14) … O(102)#4	0.93	2.71	3.569(4)	154.8
C(12)–H(12) … O(4)#5	0.93	2.64	3.186(4)	118.4

Symmetry transformations used to generate equivalent atoms: #1 −x+2,−y,−z+1 #2 −x+2,−y+1,−z #3 x−1,y+1,z #4 −x+1,−y+1,−z #5 −x+2,−y,−z.

thiazolidin-4-one ring system with similar phenyl and benzylidene substituents were found in a search of the Cambridge Crystallographic Database [58] including the archetypal 3-phenyl-5-(phenylmethylidene)-2-thioxo-1,3-thiazolidin-4-one [59]. The other related structures had substituents on either the benzene ring of the phenylmethylidene moiety [60,61] or on both benzene rings [62–66] with one instance of a phenylethylidene substituent at C5 [67].

3.3. Crystal packing for compound 1

Compound **1** crystallizes in the triclinic space group P-1 with Z = 2. In the crystal structure of **1**, C161–H16B···O101 hydrogen bonds (Table 2) link molecules into chains. These chains are linked in an obverse fashion by C8–H8···S2 and C9–H9···S2 hydrogen bonds with S2 acting as a bifurcated acceptor and these contacts link adjacent molecules forming inversion dimers, simultaneously generating $R^2_2(18)$, $R^2_2(16)$ and $R^1_2(5)$ ring motifs. Similar inversion dimers are generated on the opposite side of the molecule by C6–H6···O4 and C12–H12···O4 contacts with O4 acting as the bifurcated acceptor in this case, with the generation of $R^2_2(14)$, $R^2_2(10)$ and $R^1_2(5)$ rings and again link to an adjacent chain in an obverse fashion. This array of contacts generates layers of molecule in a plane approximately parallel to (-1 -1 3) (Fig. 2).

C15–H15···O16 contacts form additional inversion dimers and generate $R^2_2(8)$ rings and these dimers are linked by C18–H18···O4 hydrogen bonds into layers in the *ac* plane (Fig. 3). This extensive series of contacts combines to stack the molecules along the *a* axis direction (Fig. 4).

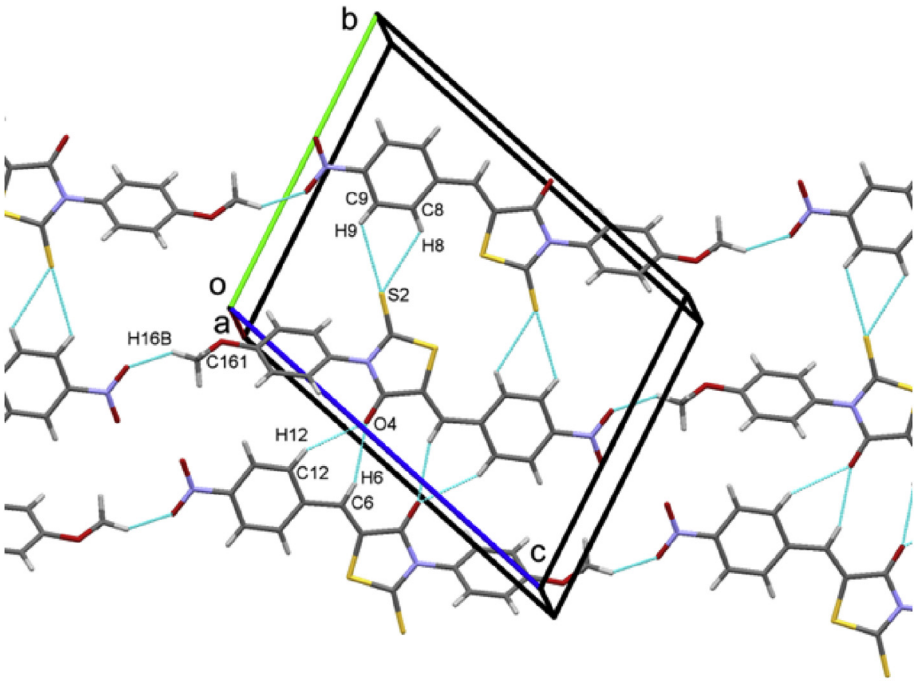

Fig. 2. Layers of molecules of **1** parallel to (-1 -1 3). In this and subsequent Figures, hydrogen bonds are drawn as blue dashed lines. (For interpretation of the references to colour in this figure legend, the reader is referred to the web version of this article.)

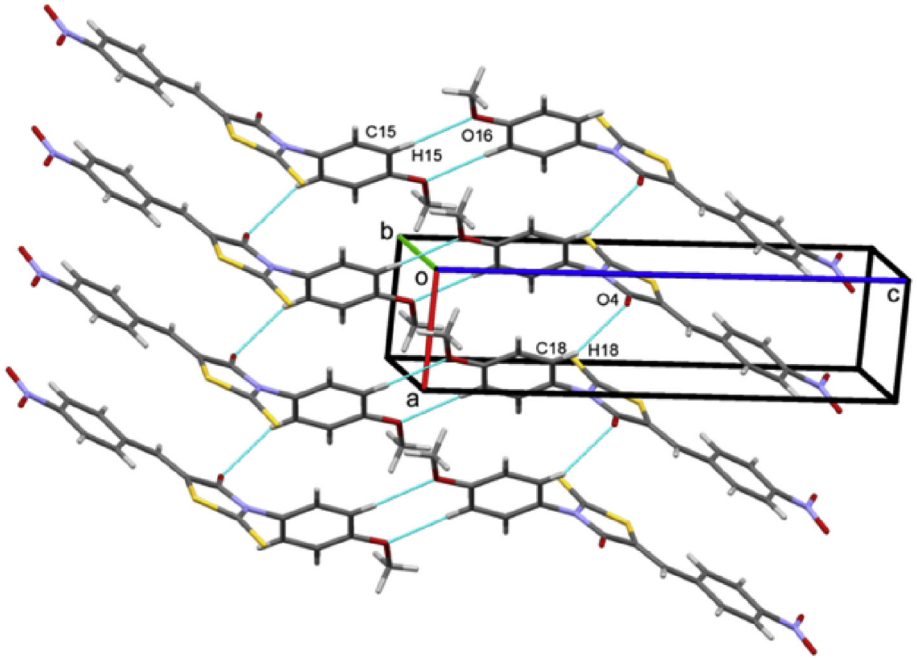

Fig. 3. Layers of inversion dimers of (**1**) in the *ac* plane.

3.4. Crystal packing for compound 2

Compound **2** also crystallizes in the triclinic space group P -1 with Z = 2. In the crystal structure of **2**, atom O102 acts as a bifurcated acceptor forming C14—H14···O102 and C18—H18···O102 hydrogen bonds (Table 3) and linking molecules in a head-to-tail fashion into sheets approximately parallel to (0 3 4). Each of these contacts also generate inversion dimers with each dimer enclosing an $R^2_2(26)$ ring motif (Fig. 5). C9—H9···O4 hydrogen bonds form chains of molecules along the *ab* diagonal (Fig. 6).

C12—H12···O4 hydrogen bonds form inversion dimers and generate $R^2_2(14)$ rings. The dimers are linked by short intermolecular S2···$S2^{2V}$ contacts, 3.4477(16) Å (2v = 2-x,-y,1-z), forming chains along *c* (Fig. 7). Overall, these contacts combine to stack the molecules along the *b* axis direction (Fig. 8).

A striking feature of the crystal structures of both molecules is

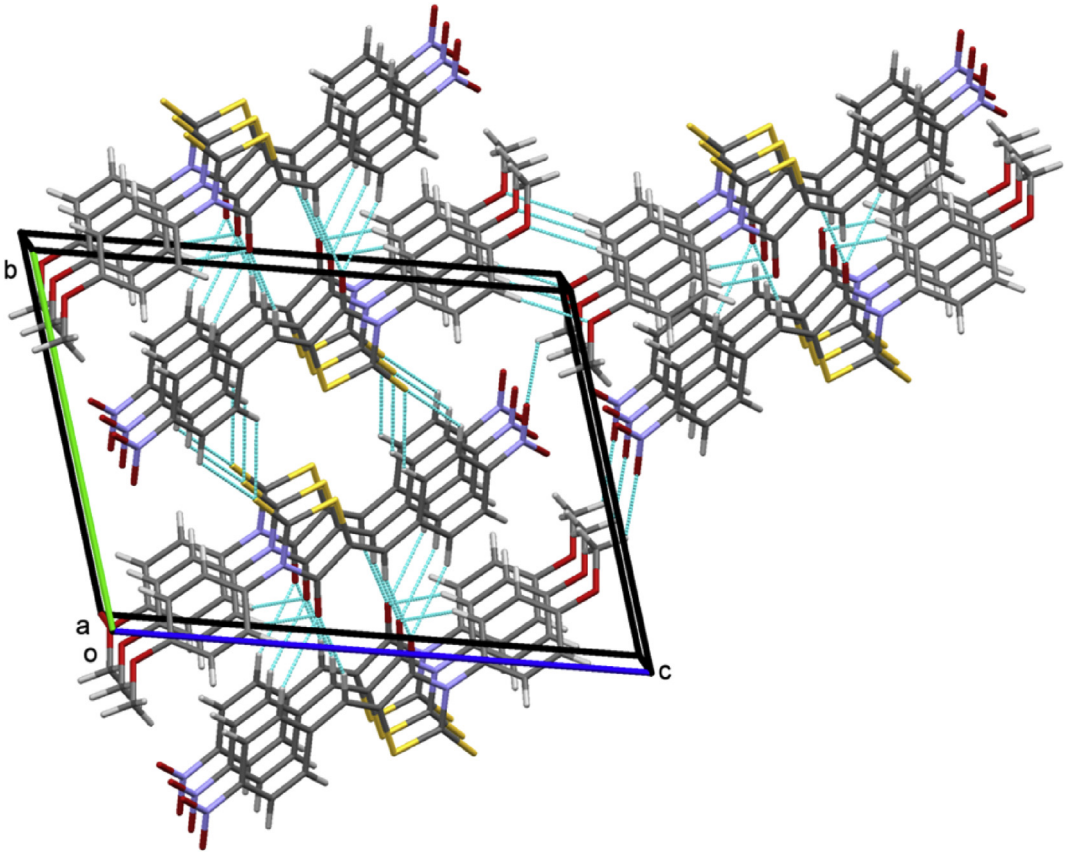

Fig. 4. Overall packing for **1** viewed along the *a* axis direction.

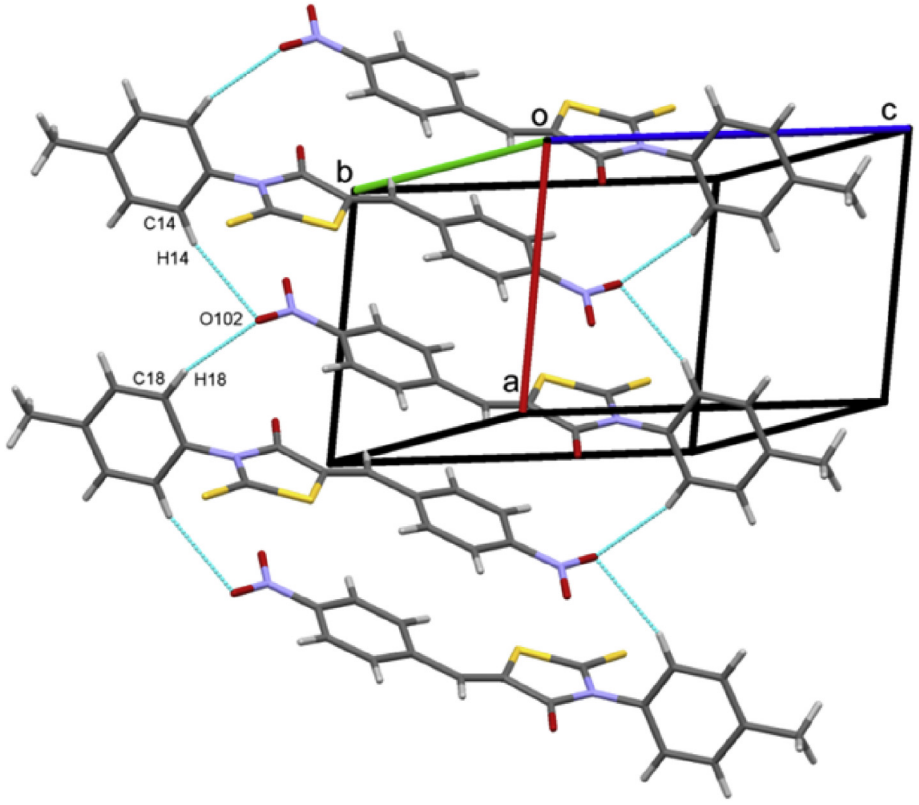

Fig. 5. Sheets of molecules of **2** parallel to (0 3 4).

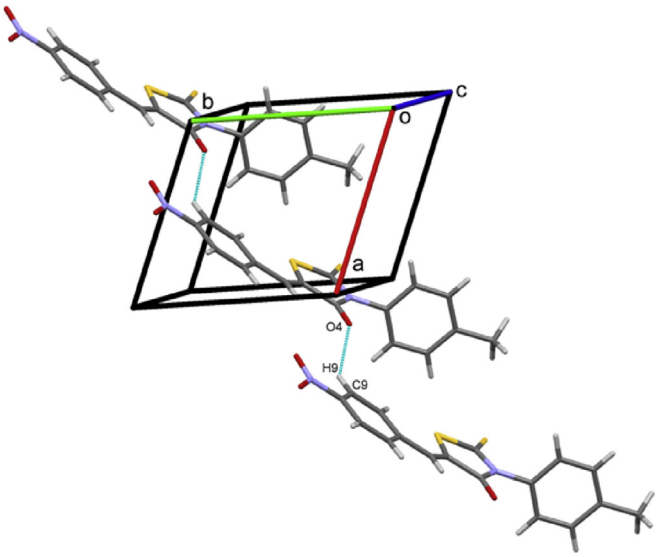

Fig. 6. C9 chains of molecules of **2** along the *ab* diagonal.

the marked tendency to form inversion dimers through non-classical C–H···S and C–H···O hydrogen bonds for **1** and C–H···O contacts for **2**.

3.5. Theoretical (DFT) study

The theoretical study is devoted to an analysis of the non-covalent interactions that are present the crystal packing of compounds **1** and **2**, excluding the H-bonding interactions that have been described in the previous section. In particular, we have focused our attention to the remarkable C–H … π, π … π interactions and lp … π-hole interactions. The importance of the C–H … π interaction in the solid state has been studied in depth by Nishio [68] and, as aforementioned, these π-hole interactions (especially those involving the nitro group) are also increasingly taken into consideration by the scientific community due to their relevance to crystal engineering and supramolecular chemistry [32–38]. Moreover, the physical nature of this type of π-hole interaction has been investigated theoretically also [69–73].

As a first approximation to rationalize the different assemblies observed in the solid state of compounds **1** and **2**, we have

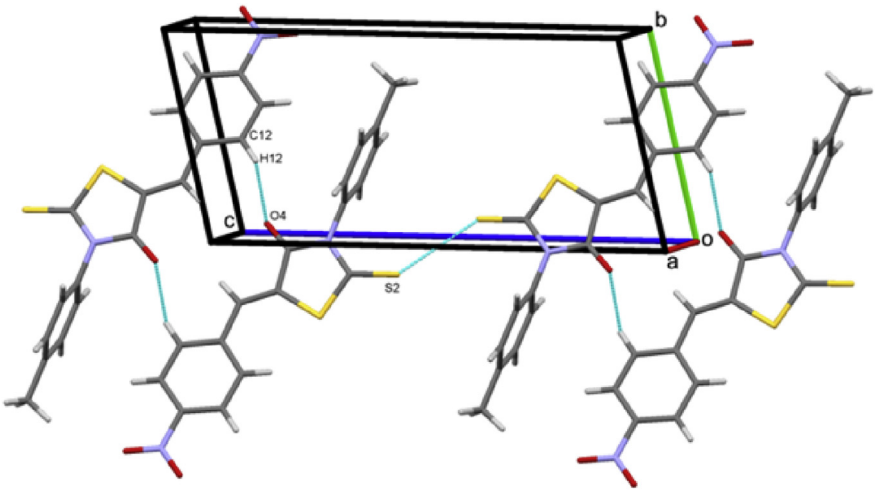

Fig. 7. Chains of inversion dimers of **2** along *c*.

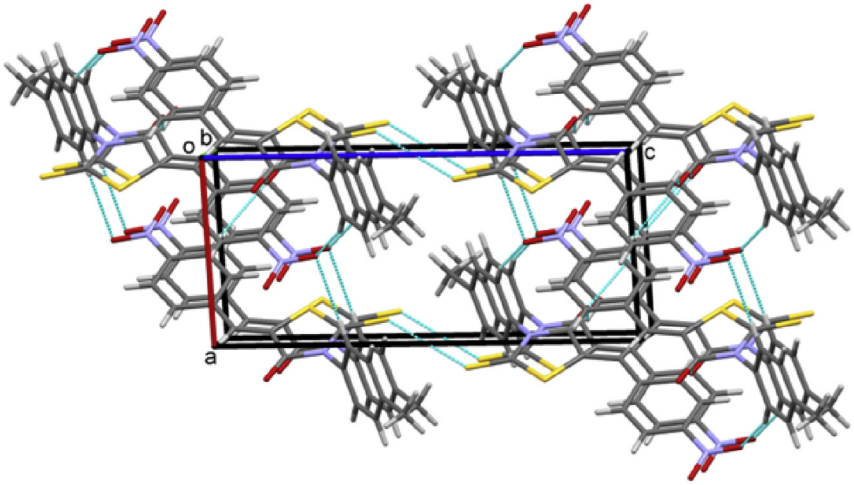

Fig. 8. Overall packing of **2** viewed along the *b* axis direction.

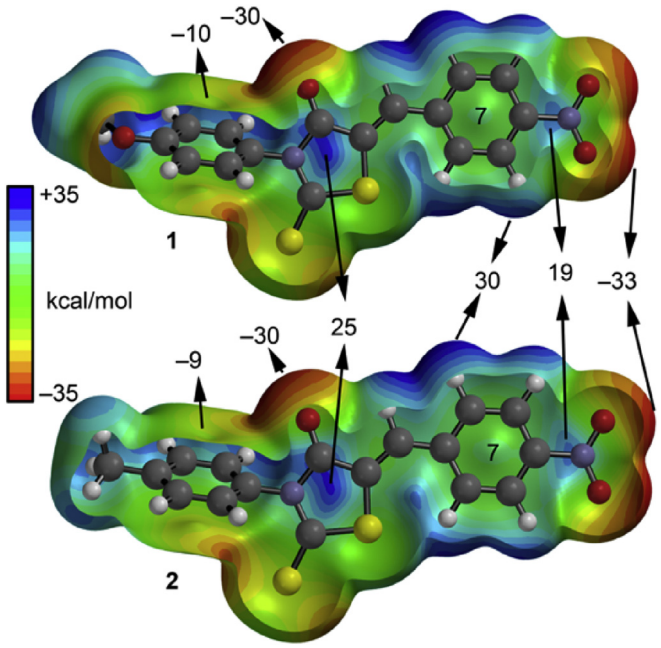

Fig. 9. Open MEP surfaces (isosurface 0.002 e/Å^3) of compounds **1** and **2**. Energies at selected points of the surfaces are given in kcal/mol.

computed their Molecular Electrostatic Potential (MEP) surfaces that are shown in Fig. 9. As expected, in both compounds the most negative regions (red surface) correspond to the oxygen atoms. The most positive region corresponds to the H atoms of the nitroarene. However, there are two π-systems that also show significantly positive (π-acidic regions). One is the five membered thioxothiazolidine ring and the other one is the π-hole over the nitro group. Interestingly, the MEP surfaces indicate that the aromatic rings present opposite electronic characteristics. That is, the *p*-nitrophenyl ring is π-acidic (+7 kcal/mol over the ring centroid) and the *p*-methoxy(or methyl)-phenyl ring is π-basic (−10 kcal/mol). Additional details of the H-bond acceptor ability of the different groups of the ligand are given in the ESI (Fig. S1).

In Fig. 10a, we illustrate a partial view of the crystal packing of compound **1** that is governed by several interactions. Basically, 2D layers are formed by H-bonding interactions that stack forming the final 3D architecture (see also Fig. 3). We have examined first the stacking mode that can be defined as a parallel-displaced arrangement (Fig. 10b). The displacement minimizes the electrostatic repulsion between the aromatic rings (the electrostatic potential over the five membered ring is very positive, Fig. 9). In fact the distance between the six membered ring centroids is large (4.21 Å) and the stacking complex formation is likely governed by other interactions involving the π-acidic regions. These include, S … π (3.69 Å) and O … π (3.57 Å) interactions involving the five membered ring and the nitro group (Fig. 10b). Moreover, a C–H···O H-bonding interaction between the methoxy groups further contributes to the stabilization of this assembly. This intricate combination of noncovalent interactions explains the large interaction energy computed for this dimer ($\Delta E_1 = -12.6$ kcal/mol). In addition, two types of self-assembled H-bonded dimers are found in the 2D layers (Fig. 10c,e). The dimer shown in Fig. 10c also presents ancillary C–H/π interactions involving the H atoms of the nitroarene (most positive H-atoms) and the π-system of the *p*-methoxyphenyl ring (electron-rich ring) in good agreement with the MEP analysis. The interaction energy of this self-assembled dimer (Fig. 10c) is $\Delta E_2 = -10.2$ kcal/mol. Furthermore we have computed the interaction energy of a theoretical dimer where the *p*-methoxyphenyl rings have been replaced by H atoms. Consequently the C–H/π interactions are not formed and the interaction energy is reduced to $\Delta E_3 = -5.4$ kcal/mol (−6.2 kcal/mol at the MP2 level) that can be attributed to the contribution of the H-bonding network (two bifurcated H-bonds) and the difference ($\Delta E_2 - \Delta E_3 = -4.8$ kcal/mol) is a rough estimation of both symmetrically equivalent C–H … π interactions. This energetic study confirms the importance of these interactions to the formation of the dimer. Finally, the other H-bonded dimer that participates in the

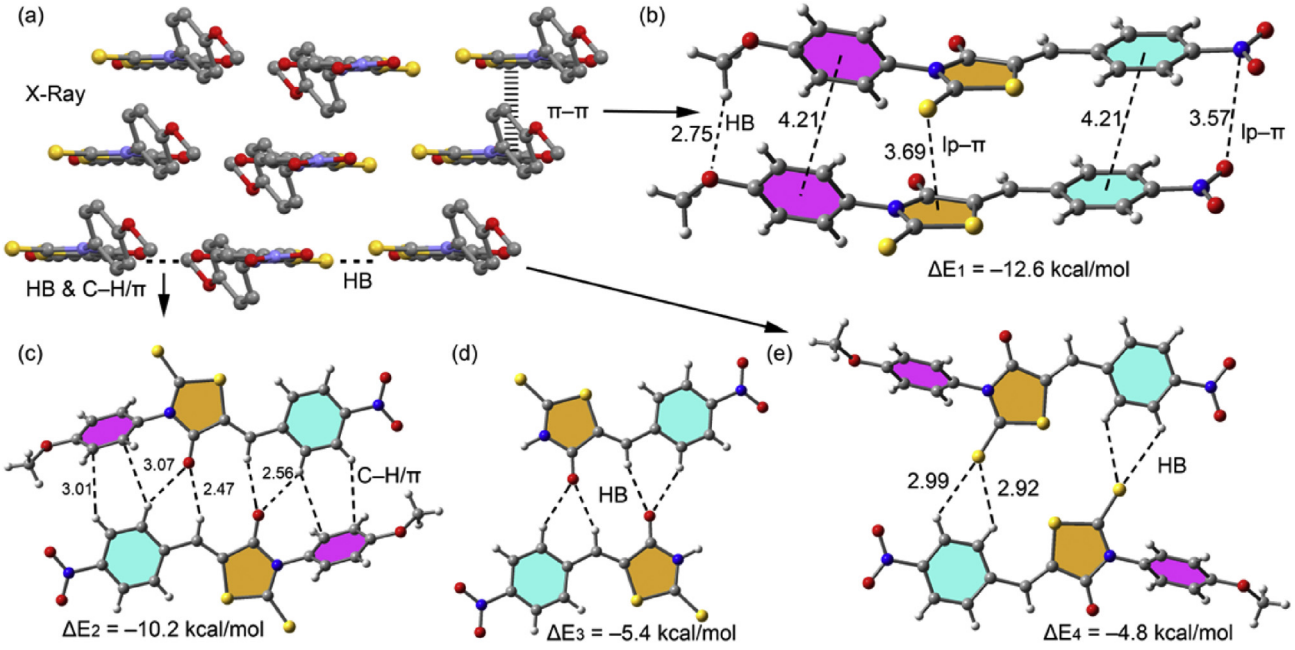

Fig. 10. (**a**) X-ray fragment of **1**, H-atoms omitted for clarity. (**b**–**e**) Theoretical models used to evaluate the π–π, H-bonding, lp–π and C–H … π interactions. Distances in Å. The π–π distance has been measured using the ring centroids.

formation of the 2D layer (Fig. 10e) presents a modest interaction energy $\Delta E_4 = -4.8$ kcal/mol (−4.4 kcal/mol at the MP2 level) because less basic S instead of O atoms participate in the formation of the bifurcated H bonds.

A similar study has been also carried out for compound **2**. In Fig. 11a, we represent a partial view of the crystal packing of this compound that is significantly different compared to that for **1**. Interestingly, the self-assembled dimer shown in Fig. 10c governed by H-bonding interactions (augmented by C–H … π interactions) in **1** is also observed in compound **2**; however, the relative importance of these two interactions is reversed. The interacting molecules are not coplanar in **2**, favoring the C–H … π interaction and weakening the H-bonds that are seen to be considerably longer (Fig. 11b). The interaction energy of this dimer is $\Delta E_5 = -9.4$ kcal/mol (similar to ΔE_5) but this is reduced to $\Delta E_6 = -2.8$ kcal/mol when an additional theoretical model is used, replacing the *p*-methylphenyl moiety by an H atom. This result confirms that this dimer is mainly governed by the C–H … π interaction since the contribution of the H-bonding interactions is only −2.8 kcal/mol. An important difference with compound **1** is the π–π stacking arrangement. In **2**, an antiparallel displaced arrangement (Fig. 11c) is observed instead of the parallel one described above. This is likely due to the absence of the methoxy group in **2** (the H-bond shown in Fig. 10b cannot be formed). Similar to **1**, the π-stacking antiparallel displacement allows the formation of two symmetrically related lp–π interactions involving the π-hole of the nitro group (3.61 Å). Moreover, this dimer is also stabilized by two H-bonds involving the aromatic H atoms and the O atoms of the nitro groups (2.53 Å). The interaction energy of this assembly is $\Delta E_7 = -10.7$ kcal/mol that is reduced to $\Delta E_8 = -8.4$ kcal/mol when the *p*-methylphenyl moieties are eliminated. Thus, the H-bonding interactions contribute −2.3 kcal/mol and the main contribution is due to a combination of lp–π and π–π interactions.

We have used Bader's theory of "atoms in molecules" (AIM) to characterize the noncovalent bonds described above for complex **1** as a model system. A bond critical point (CP) and a bond path connecting two atoms is unambiguous evidence of interaction. The AIM distribution of critical points and bond paths computed for two dimers of compound **1** is shown in Fig. 12. The distribution in the self-assembled H-bonded dimer (with ancillary C–H … π interactions) reveals that each bifurcated H-bond is characterized by two CPs (red spheres) and bond paths connecting the O atom with two H atoms (Fig. 12a). The C–H … π interaction is characterized by two CPs (red spheres) and bond paths connecting the C–H bonds to two C atoms of the arene. Finally, the AIM analysis also reveals the formation of two symmetrically equivalent H-bonds between the nitro and methoxy groups characterized by a bond CP and a bond path. The distribution of CPs and bond paths for the parallel displaced π-stacking complex is shown in Fig. 12b. All interactions described above in the energetic study (π–π, lp–π and H-bonding interactions) are confirmed by the AIM analysis. They are characterized by the presence of a bond CP and a bond path connecting the electron-rich atom with the corresponding H atom in the case of H-bonding interactions or with a C/S atom for the π-interactions (π–π or lp–π).

Finally, we have used the noncovalent interaction plot (NCIplot) analysis for the dimers analyzed above. As described in the literature, this approach is a computational tool based on the electron density and its derivatives [53]. The peaks that appear in the reduced density gradient (s) at low densities correspond to the different noncovalent interactions. The sign of the second eigenvalue (λ_2) of the electron-density Hessian matrix is used to distinguish bonded ($\lambda_2 < 0$) from nonbonded ($\lambda_2 > 0$) interactions and its strength can be derived from the density values of the low-gradient spikes. An advantage of this method is the visualization in real space of the gradient isosurfaces. Fig. 13 displays the NCI

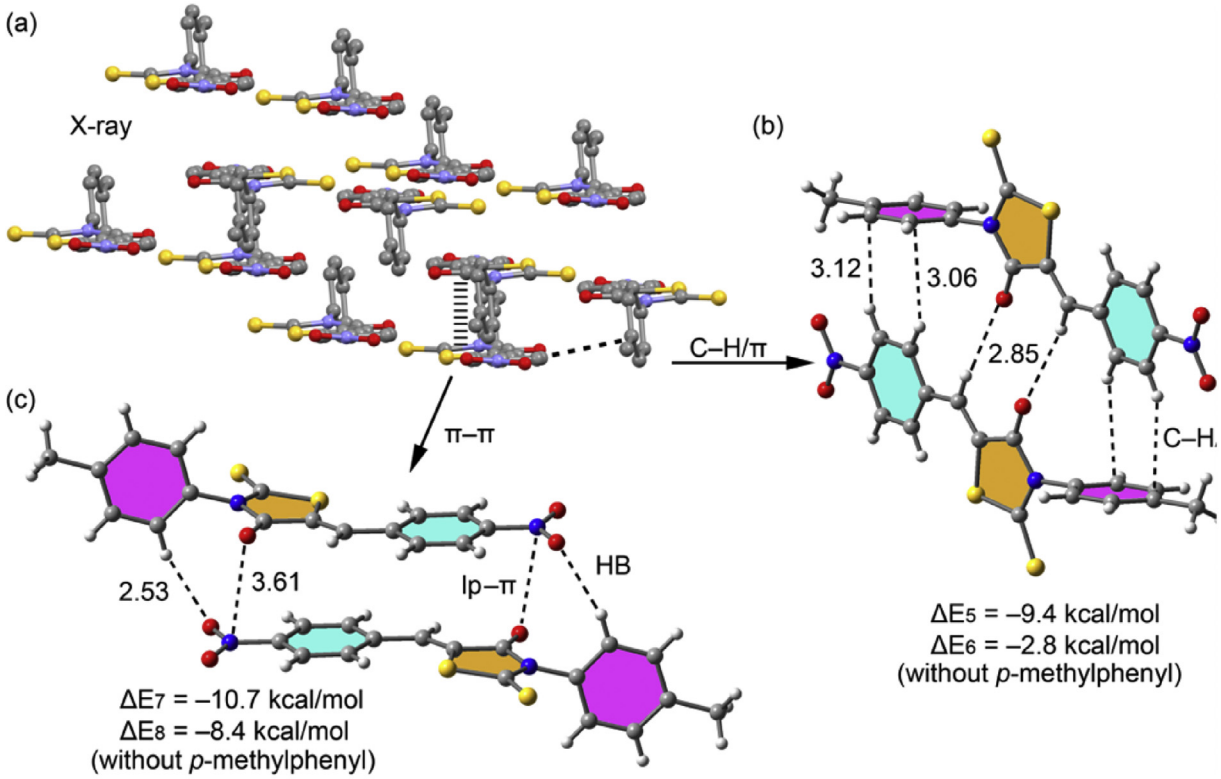

Fig. 11. (**a**) X-ray fragment of **2**. (**b**–**c**) Theoretical models used to evaluate the C–H … π, lp … π and H-bonding interactions. Distances in Å.

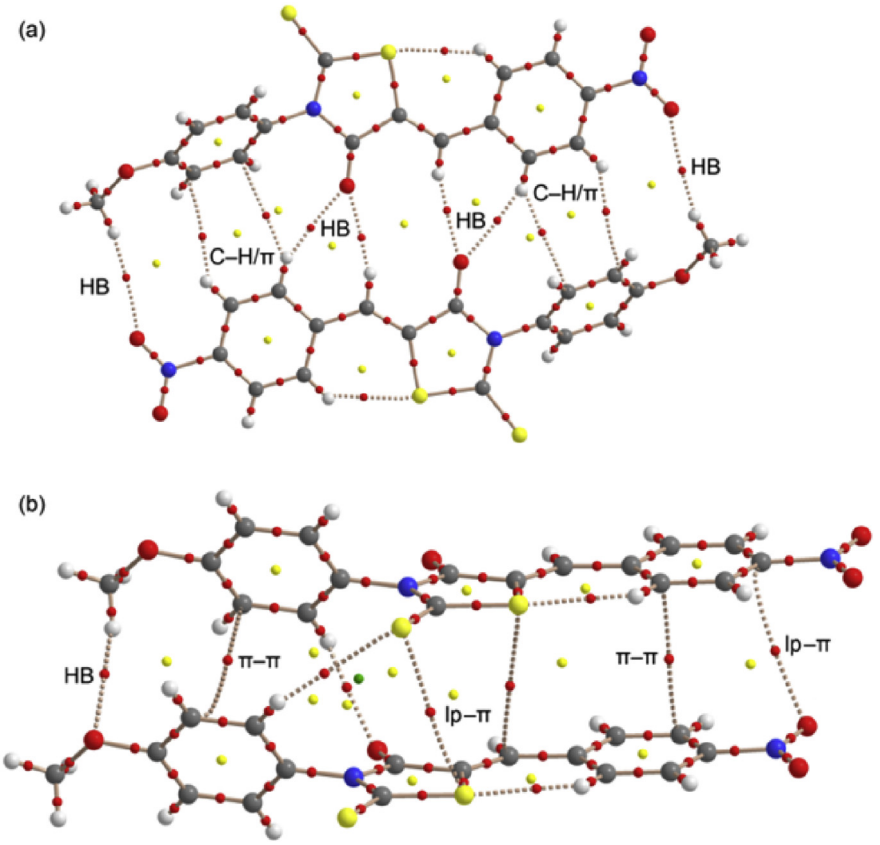

Fig. 12. Distribution of bond, ring and cage critical points (red, yellow and green spheres, respectively) and bond paths for two dimers of compound **1**. (For interpretation of the references to colour in this figure legend, the reader is referred to the web version of this article.)

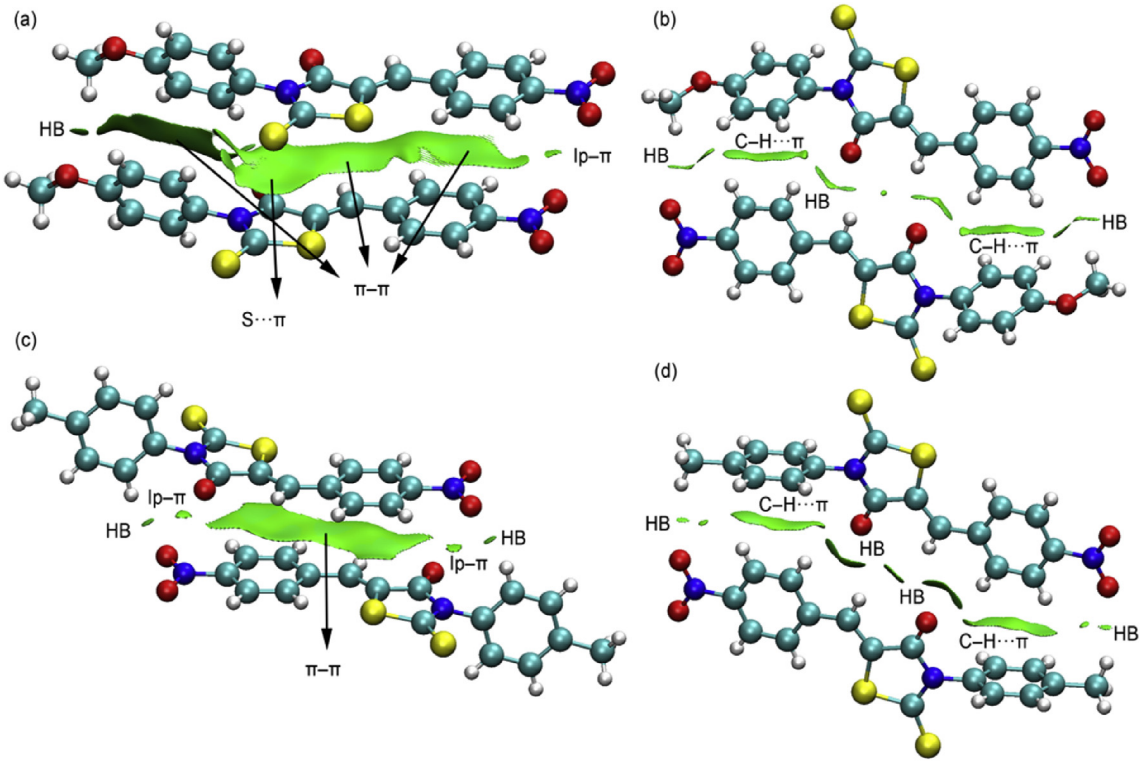

Fig. 13. NCI analysis of complexes **1**, (a,b) and **2** (c,d). The gradient isosurfaces are colored on a BGR scale according to the sign $(\lambda_2)\rho$ over the range −0.015 to 0.015 a.u.

isosurfaces of the dimers of complexes **1** (a,b) and **2** (b,c) obtained to visualize the H-bonding, lp–π, π–π and C–H … π interactions. The noncovalent interaction peaks appear at density values lower than 0.01 a.u., which corresponds to the region of weak interactions, characterized by the green color at the isosurfaces. In all dimers the color observed for the isosurface area is green, remarking the attractive nature of the interaction. Interestingly for compound **1** (Fig. 13a and b) the π–π stacking is characterized by a large isosurface that is extended to the three rings of the ligand and the conjugated double bond. The other interactions are characterized by smaller isosurfaces due to the smaller overlap of the interacting atoms and the higher directionality of the interaction. For compound **2**, the NCIplot also reveals a large isosurface that corresponds to the π–π stacking (see Fig. 13c) and smaller isosurfaces that characterize the rest of the interactions. Remarkably, for both compounds **1** and **2** the lp–p interaction involving the p-hole of the nitro group has been confirmed by the presence of a small isosurface in the middle of the O and N atoms that participate in the interaction.

3.6. Conclusions

Two new 3-aryl-5-(4-nitrobenzylidene)-2-thioxothiazolidin-4-one derivatives (**1** & **2**) were successfully synthesized and characterized by FT-IR, NMR spectroscopy, elemental analysis and single-crystal X-ray diffraction studies. These new organic compounds present interesting noncovalent interactions in their crystal packing, including lp … π interactions where both the π–holes of the thioxothiazolidinone ring and the nitro group act as Lewis acids. The energetic features of these interactions have been studied by means of high level DFT calculations and evaluated energetically. Finally, these new types of interactions might be rationally utilized in crystal engineering, much like the σ-hole interactions found with hydrogen and halogen bonding.

Acknowledgements

H.A. is grateful to the Higher Education Commission, Pakistan for financial support under Indigenous 5000 Ph.D Fellowship program. J.S. thanks the Chemistry Department, University of Otago for support of his work. A.B. and A.F. thank DGICYT of Spain (project CTQ2014-57393-C2-1-P) for funding. We thank the CTI (UIB) for free allocation of computer time.

Appendix A. Supplementary data

Supplementary data related to this article can be found at http://dx.doi.org/10.1016/j.molstruc.2017.03.046.

References

[1] K. Hajibabaei, Synlett (2014) 2083–2084.
[2] M.E. Welsch, S.A. Snyder, B.R. Stockwell, Curr. Opin. Chem. Biol. 14 (2010) 347–361.
[3] T. Tomasic, L.P. Masic, Curr. Med. Chem. 16 (2009) 1596–1629.
[4] R. Maccari, R. Ottana, C. Curinga, M.G. Vigorita, D. Rakowitz, T. Steindl, T. Langer, Bioorg. Med. Chem. 13 (2005) 2809–2823.
[5] E.B. Grant, D. Guiadeen, E.Z. Baum, B.D. Foleno, H. Jin, D.A. Montenegro, E.A. Nelson, K. Bush, D.J. Hlasta, Bioorg. Med. Chem. Lett. 10 (2000) 2179–2182.
[6] W.T. Sign, C.L. Lee, S.L. Yeo, S.P. Lim, M.M. Sim, Bioorg. Med. Chem. Lett. 11 (2001) 91–94.
[7] C.A. Free, E. Majchrowicz, S.M. Hess, Biochem. Pharmacol. 20 (1971) 1421–1428.
[8] L.M. Szewczuk, S.A. Saldanha, S. Ganguly, E.M. Bowers, M. Javoroncov, B. Karanam, J.C. Culhane, M.A. Holbert, D.C. Klein, R. Abagyan, P.A. Cole, J. Med. Chem. 50 (2007) 5330–5338.
[9] S.D. Furdas, S. Shekfeh, S. Kannan, W. Sippl, M. Jung, Med. Chem. Commun. 3 (2012) 305–311.
[10] Ş.H. Üngören, S. Albayrak, A. Günay, L. Yurtseven, N. Yurttaş, Tetrahedron 71 (2015) 4312–4323.
[11] R. Bryk, B. Gold, A. Venugopal, J. Singh, R. Samy, K. Pupek, H. Cao, C. Popescu, M. Gurney, S. Hotha, J. Cherian, K. Rhee, L. Ly, P.J. Converse, S. Ehrt, O. Vandal, X. Jiang, J. Schneider, G. Lin, C. Nathan, Cell Host Microbe 3 (2008) 137–145.
[12] M. Sortino, P. Delgado, S. Juárez, J. Quiroga, R. Abonia, B. Insuasty, M. Nogueras, L. Rodero, F.M. Garibotto, R.D. Enriz, S.A. Zacchino, Bioorg. Med. Chem. 15 (2007) 484–494.
[13] M.G. Orchard, J.C. Neuss, C.M.S. Galley, A. Carr, D.W. Porter, P. Smith, D.I.C. Scopes, D. Haydon, R. Vousden, C.R. Stubberfield, K. Young, M. Page, Bioorg. Med. Chem. Lett. 14 (2004) 3975–3978.
[14] J. Dolezel, P. Hirsova, V. Opletalova, J. Dohnal, V. Marcela, J. Kunes, J. Jampilek, Molecules 14 (2009) 4197–4212.
[15] A.J. Russel, I.M. Westwood, M.H.J. Crawford, J. Robinson, A. Kawamura, C. Redfield, N. Laurieri, E.D. Lowe, S.G. Davies, E. Sim, Bioorg. Med. Chem. 17 (2009) 905–918.
[16] S. Breuer, M.W. Chang, J. Yuan, B.E. Torbett, J. Med. Chem. 55 (2012) 4968–4977.
[17] K. Chauhan, M. Sharma, P. Singh, V. Kumar, P.K. Shukla, M.I. Siddiqi, P.M.S. Chauhan, Med. Chem. Commun. 3 (2012) 1104–1110.
[18] P. Shah, T.M. Dhameliya, R. Bansal, M. Nautiyal, D.N. Kommi, P.S. Jadhavar, J.P. Sridevi, P. Yogeeswari, D. Sriram, A.K. Chakraborti, Med. Chem. Commun. 5 (2014) 1489–1495.
[19] T. Ollevier, Org. Biomol. Chem. 11 (2013) 2740–2755.
[20] F. Xue, A.D. MacKerell Jr., G. Heinzl, K. Hom, Tetrahedron Lett. 54 (2013) 1700–1703.
[21] V. Ramesh, B.A. Rao, P. Sharma, B. Swarna, D. Thummuri, K. Srinivas, V.G.M. Naidu, V.J. Rao, Eur. J. Med. Chem. 83 (2014) 569–580.
[22] A. Mishra, M.K.R. Fischer, P. Bauerle, Angew. Chem. Int. Ed. 48 (2009) 2474–2499.
[23] L. Dalton, Adv. Polym. Sci. 158 (2002) 1–86.
[24] A.K.Y. Jen, T.A. Chen, V.P. Rao, Y. Cai, Y.J. Liu, L.R. Dalton, Adv. Nonlinear Opt. 4 (1997) 237–249.
[25] J.M. Lehn, Supramolecular Chemistry: Concepts and Perspectives, first ed., Wiley VCH, Weinheim, 1995.
[26] H.J. Schneider, Supramolecular Systems in Biomedical Fields, first ed., RSC Publishing, Cambridge, UK, 2013.
[27] A.W. Steed, J.L. Atwood, Supramolecular Chemistry, first ed., John Wily & Sons, Ltd., Chichester, UK, 2009.
[28] P.J. Cragg, Supramolecular Chemistry: from Biological Inspiration to Biomedical Applications, first ed., Springer, Dordrecht, 2010.
[29] T. Clark, WIREs Comput. Mol. Sci. 3 (2013) 13–20.
[30] P. Politzer, J.S. Murray, T. Clark, Phys. Chem. Chem. Phys. 15 (2013) 11178–11189.
[31] P. Politzer, J.S. Murray, P. Lane, Int. J. Quantum Chem. 107 (2007) 3046–3052.
[32] A. Bauza, T.J. Mooibroek, A. Frontera, Chem. Commun. 51 (2015) 1491–1493.
[33] A. Bauza, T.J. Mooibroek, A. Frontera, ChemPhysChem 16 (2015) 2496–2517.
[34] A. Bauza, T.J. Mooibroek, A. Frontera, Chem. Rec. 16 (2016) 473–487.
[35] J.S. Murray, P. Lane, T. Clark, K.E. Riley, P. Politzer, J. Mol. Model. 18 (2012) 541–548.
[36] T.J. Mooibroek, P. Gamez, CrystEngComm 14 (2012) 1027–1030.
[37] T.J. Mooibroek, P. Gamez, CrystEngComm 14 (2012) 3902–3906.
[38] A. Bauza, A. Frontera, T.J. Mooibroek, Cryst. Growth Des. 16 (2016) 5520–5524.
[39] H. Andleeb, Y. Tehseen, S.J.A. Shah, I. Khan, J. Iqbal, S. Hameed, RSC Adv. 6 (2016) 77688–77700.
[40] C. Nitsche, C.D. Klein, Tetrahedron Lett. 53 (2012) 5197–5201.
[41] Bruker APEX2, SAINT and SADABS, Bruker AXS Inc., Madison, Wisconsin, USA, 2011.
[42] G.M. Sheldrick, Acta Crystallogr. Sect. A Found. Crystallogr. A64 (2008) 112–122.
[43] G.M. Sheldrick, Acta Crystallogr. Sect. C. Cryst. Struct. Commun. 71 (2015) 3–8.
[44] C.F. Macrae, I.J. Bruno, J.A. Chisholm, P.R. Edgington, P. McCabe, E. Pidcock, L. Rodriguez-Monge, R. Taylor, J. van de Streek, P.A. Wood, J. Appl. Cryst. 41 (2008) 466–470.
[45] A.L. Spek, Acta Crystallogr. Sect. D. Biol. Crystallogr. D65 (2009) 148–155.
[46] L.J. Farrugia, J. Appl. Cryst. 45 (2012) 849–854.
[47] R. Ahlrichs, M. Bär, M. Häser, H. Horn, C. Kölmel, Chem. Phys. Lett. 162 (1989) 165–169.
[48] (a) A. Bauzá, A. Terrón, M. Barceló-Oliver, A. García-Raso, A. Frontera, Inorg. Chim. Acta. (2015), http://dx.doi.org/10.1016/j.ica.2015.04.028;
(b) D. Sadhukhan, M. Maiti, G. Pilet, A. Bauzá, A. Frontera, S. Mitra, Eur. J. Inorg. Chem. 11 (2015) 1958–1972;
(c) M. Mirzaei, H. Eshtiagh-Hosseini, Z. Bolouri, Z. Rahmati, A. Esmaeilzadeh, A. Hassanpoor, A. Bauza, P. Ballester, M. Barceló-Oliver, J.T. Mague, B. Notash, A. Frontera, Cryst. Growth Des. 15 (2015) 1351–1361;
(d) P. Chakraborty, S. Purkait, S. Mondal, A. Bauzá, A. Frontera, C. Massera, D. Das, CrystEngComm 17 (2015) 4680–4690.
[49] S.F. Boys, F. Bernardi, Mol. Phys. 19 (1970) 553–566.
[50] R.F.W. Bader, Atoms in Molecules - a Quantum Theory, Oxford University Press, Oxford, U.K., 1990.
[51] T.A. Keith, AIMAll (Version 13.05.06), T. K. Gristmill Software, Overland Park KS, USA, 2013.
[52] Y. Shao, L.F. Molnar, Y. Jung, J. Kussmann, C. Ochsenfeld, S.T. Brown,

A.T.B. Gilbert, L.V. Slipchenko, S.V. Levchenko, D.P. O'Neill, R.A. DiStasio Jr., R.C. Lochan, T. Wang, G.J.O. Beran, N.A. Besley, J.M. Herbert, C.Y. Lin, T. Van Voorhis, S.H. Chien, A. Sodt, R.P. Steele, V.A. Rassolov, P.E. Maslen, P.P. Korambath, R.D. Adamson, B. Austin, J. Baker, E.F.C. Byrd, H. Dachsel, R.J. Doerksen, A. Dreuw, B.D. Dunietz, A.D. Dutoi, T.R. Furlani, S.R. Gwaltney, A. Heyden, S. Hirata, C.-P. Hsu, G. Kedziora, R.Z. Khalliulin, P. Klunzinger, A.M. Lee, M.S. Lee, W.Z. Liang, I. Lotan, N. Nair, B. Peters, E.I. Proynov, P.A. Pieniazek, Y.M. Rhee, J. Ritchie, E. Rosta, C.D. Sherrill, A.C. Simmonett, J.E. Subotnik, H.L. Woodcock III, W. Zhang, A.T. Bell, A.K. Chakraborty, D.M. Chipman, F.J. Keil, A. Warshel, W.J. Hehre, H.F. Schaefer, J. Kong, A.I. Krylov, P.M.W. Gill, M. Head-Gordon, Phys. Chem. Chem. Phys. 8 (2006) 3172–3191.

[53] J. Contreras-Garcia, E.R. Johnson, S. Keinan, R. Chaudret, J.-P. Piquemal, D.N. Beratan, W. Yang, J. Chem. Theory Comput. 7 (2011) 625–632.

[54] P. Mandal, Mithuna, A. Garg, S.S. Sahetya, S.R. Nagendra, H.S. Sripad, M.M. Manjunath, Sitaram, Mukesh Soni, R.N. Baig, S.V. Kumar, B.R.P. Kumar, RSC Adv. 6 (2016) 58641–58653.

[55] W.T. Sing, C.L. Lee, S.L. Yeo, S.P. Lim, M.M. Sim, Bioorg. Med. Chem. Lett. 11 (2001) 91–94.

[56] A.I. Khodair, J. Heterocyc. Chem. 39 (2002) 1153–1160.

[57] Y. Ohishi, T. Mukai, M. Nagahara, M. Yajima, N. Kajikawa, K. Miahara, T. Takano, Chem. Pharm. Bull. 38 (1990) 1911–1919.

[58] C.R. Groom, I.J. Bruno, M.P. Lightfoot, S.C. Ward, Acta Cryst. B72 (2016) 171–179.

[59] A. Linden, E.M.A.H. Awad, H. Heimgartner, Acta Crystallogr. Sect. C. Cryst. Struct. Commun. 55 (1999) 1877–1881.

[60] D. Shahwar, M.N. Tahir, M.A. Raza, B. Iqbal, Acta Crystallogr. Sect. E Struct. Rep. Online 65 (2009) o2903.

[61] D. Shahwar, M.N. Tahir, M.A. Raza, B. Iqbal, Acta Crystallogr. Sect. E Struct. Rep. Online 65 (2009) o2917.

[62] N. Benhalima, K. Toubal, A. Chouaih, G. Chita, S. Maggi, A. Djafri, F. Hamzaoui, J. Chem. Cryst. 41 (2011) 1729–1736.

[63] N. Benhalima, K. Toubal, A. Chouaih, G. Chita, S. Maggi, A. Djafri, F. Hamzaoui, Molecules 17 (2012) 3501–3509.

[64] M. Ashraf, A. Teshome, A.J. Kay, G.J. Gainsford, M.D.H. Bhuiyan, I. Asselberghs, K. Clays, Dyes Pigm. 98 (2013) 82–92.

[65] C. Abdelkader, CSD Commun. Priv. Commun. (2015).

[66] D. Shahwar, M.N. Tahir, M. Kashif, A. Saeed, S. Bukhari, Acta Crystallogr. Sect. E Struct. Rep. Online 68 (2012) o1818.

[67] M.S. Seyfried, A. Linden, G. Mloston, H. Heimgartner, Helv. Chim. Acta 92 (2009) 1800–1816.

[68] M. Nishio, CrystEngComm 6 (2004) 130–158.

[69] A. Bauza, R. Ramis, A. Frontera, J. Phys. Chem. A 118 (2014) 2827–2834.

[70] M. Solimannejad, V. Ramezani, C. Trujillo, I. Alkorta, G. Sanchez-Sanz, J. Elguero, J. Phys. Chem. A 116 (2012) 5199–5206.

[71] C. Trujillo, G. Sanchez-Sanz, I. Alkorta, J. Elguero, New J. Chem. 39 (2015) 6791–6802.

[72] G. Sanchez-Sanz, C. Trujillo, M. Solimannejad, I. Alkorta, J. Elguero, Phys. Chem. Chem. Phys. 15 (2013) 14310–14318.

[73] A. Bauzá, A. Frontera, T. Mooibroek, Nat. Commun. 8 (2017) 14522.